ARTICLE

BIOTECHNOLOGY and BIOENGINEERING

Cellulose Hydrolysis in Evolving Substrate Morphologies III: Time-Scale Analysis

Wen Zhou,[1,2] Ying Xu,[1,2] Heinz-Bernd Schüttler[3]

[1]Computational Systems Biology Lab, Department of Biochemistry and Molecular Biology, Institute of Bioinformatics, University of Georgia, Athens, Georgia; telephone: 706-542-9779; fax: 706-542-9751; e-mail: xyn@bmb.uga.edu

[2]BioEnergy Science Center (BESC), Department of Energy (DOE), Oak Ridge, Tennessee

[3]Department of Physics and Astronomy, University of Georgia, Athens, Georgia; telephone: 706-542-3886; fax: 706-542-2492; e-mail: hbs@physast.uga.edu

Received 11 December 2009; revision received 4 May 2010; accepted 10 May 2010

Published online 1 June 2010 in Wiley Online Library (wileyonlinelibrary.com). DOI 10.1002/bit.22814

ABSTRACT: We present a time-scale analysis for the enzymatic hydrolysis of solid cellulosic substrates, based on our recently developed kinetic model (Zhou et al., 2009a, Biotechnol Bioeng 104:261–274; Zhou et al., 2009b, Biotechnol Bioeng 104:275–289) which incorporates both enzymatic chain fragmentation and hydrolytic time evolution of the solid substrate morphology. Analytical order-of-magnitude estimates of the relevant single-layer chain depolymerization times are first discussed. These time-scale estimates for pure and mixed enzyme systems can be employed to calculate the degree of synergy between *endo*- and *exo*-acting enzymes in a mixed enzyme system. By the way of a quasi-steady-state approximation which allows for a greatly simplified analytical solution of the model, we also explain the origin and give order-of-magnitude estimates of the two characteristic hydrolysis time scales which arise in this model when the solid substrate morphology is taken into account. These analytically derived time-scale relations explain how the embedding of cellulose chains in a solid substrate acts as a crucial rate-limiting factor and results in a substantial slowing down of the hydrolytic conversion process, compared to a hypothetical substrate of immediately enzyme-accessible, isolated chains. The analytical time-scale results are verified by numerical simulations and compared to experimental observations.

Biotechnol. Bioeng. 2010;107: 224–234.

KEYWORDS: cellulose hydrolysis; substrate morphology; mathematical model; time-scale analysis; degree of synergy

Introduction

The conversion of cellulosic biomass to biofuel has the potential to replace a substantial amount of fossil transportation fuel in the foreseeable future, because of the availability of the large quantities of plant biomass. To realize this potential and to advance the development of cost-effective and energy-efficient biofuel production process, modeling and process simulation are critical. In two recent companion articles, referred to as I (Zhou et al., 2009a) and II (Zhou et al., 2009b), respectively, we have developed a general framework for realistic modeling of enzymatic hydrolysis kinetics for solid substrates being fragmentized and solubilized by free (i.e., non-microbe-bound) cellulases. Within this general framework, developed in I, we explicitly account for the hydrolytic evolution of substrate morphology, which is driven by the solubilization and fragmentation of cellulose chains exposed to enzyme attack on internal and external solid substrate surfaces. This framework goes beyond the most advanced previous non-morphologic modeling efforts (Converse and Optekar, 1993; Fenske et al., 1999; Okazaki and Moo-Young, 1978; Suga et al., 1975; Zhang and Lynd, 2006), which consider cellulose chains only in complete isolation, without their collective embedding and mutual obstruction in the solid. The non-morphologic models can therefore only describe the very earliest stage of the hydrolytic conversion process. In II, we have applied our kinetic modeling framework to a real cellulose hydrolysis experimental system employing cellulase mixtures of the model cellulolytic micro-organism *Trichoderma reesei* on the model cellulosic substrate Avicel. The numerical simulation results are consistent with previously reported experiments and can reproduce some important experimental features, such as the hydrolysis slow down. These numerical results thus provide useful information, which can be further experimentally tested, on the mechanism of the interaction between enzymes and substrate during the hydrolytic digestion.

In the present work, we carry out a theoretical analysis based on the "five-site" model developed in II. Specifically,

Correspondence to: H.-B. Schüttler and Y. Xu

Additional Supporting Information may be found in the online version of this article.

our analysis focuses on the time it takes to hydrolyze most or a substantial fraction of the substrate. From an engineering point of view, the time to complete solubilization is a critical process indicator and it usually determines the size and volume of the corresponding process equipment. We show that the time scales estimated through our theoretical analysis and certain analytical approximations to the model of II are in good agreement with the numerical simulation results, and the resulting simple formulae reveal critical parameter dependencies of the process that have been observed in experiments. We also present an expression for the degree of synergy (DS) for mixed enzyme systems, containing both *exo*- and *endo*-acting cellulases, based on time scales only. Mathematical notation and abbreviations used here are fully consistent with nomenclatures of articles I and II. New symbols and abbreviations introduced here are defined first in the context. All symbols and abbreviations that appear in this article are summarized in the nomenclature.

Materials and Methods

We consider a substrate of pure cellulose in its solid form. Other non-cellulosic components, such as lignin, hemicellulose, and pectin, are assumed to have been either digested, or removed/redistributed, in a separate pretreatment process, such that they no longer obstruct the cellulose hydrolysis (e.g., Avicel, filter paper). These substrates are characterized by different degrees of polymerization (DP) and different fractions ($\overline{F}_a$) of β(1,4)-glucosidic bonds surface accessible to cellulase. For instance, typical Avicel has a DP value around 300 and $\overline{F}_a$ of 0.006 (Zhang and Lynd, 2004). We also assume initial chain lengths ℓ, that is, an initial DP-value, satisfying the long chain limit (LCL) assumption, $\ell = \mathrm{DP}^{(o)} \gg \ell_S$, where ℓ_S is the minimum insoluble glucan chain length of typically 4–7 monomers (Stalbrand et al., 1998). As in II, we use $\ell_S = 7$ for all numerical calculations. All calculations reported here are based on the *T. reesei* three-enzyme system, comprising two exoglucanases, cellobiohydrolases CBH1 and CBH2, and an endoglucanase EG1 (Goyal et al., 1991). Similar enzyme systems can be found in other aerobic fungi and bacteria, such as other *Trichoderma* species and *Thermobifida fusca*. All enzyme kinetics and substrate model parameters used here are the same as given in Table I of II, unless stated otherwise. Molar concentrations of the "E1" system defined in II are denoted here by $[\mathrm{EG1}]^{(o)}$, $[\mathrm{CBH1}]^{(o)}$, and $[\mathrm{CBH2}]^{(o)}$.

The mathematical representation of our general modeling framework (in both a "site number" and a "chain number" formalism), and its applications to the "five-site" model are given in the model development section and in the Supporting Information (SI) Sections A–H of I and in the SI Sections A–C of II, respectively. Central concepts in this formalism are (i) the characterization of all β(1,4) glucosidic bonds along the cellulose chain in terms of a "site type"; (ii) the sub-division of the solid substrate into the so-called "smallest accessible compartments" (SACs); (iii) the sub-division of SACs into "layers" of successive hydrolytic ablation; and (iv) the modeling of a heterogeneous substrate morphology in terms of SAC "geometry classes," labeled by a class index σ and quantified by continuous time-evolving SAC size variables, $\lambda_\sigma(t)$.

Our time-scale analysis is based on cutting rate factors $\Gamma_{N,\sigma}$, $\Gamma_{X,\sigma}$, and $\Gamma_{Y,\sigma}$, constructed in II, SI Section A, from enzyme-bond cutting rate coefficients (γ), enzyme–substrate adsorption coefficients (L), total enzyme concentrations (u), and molar concentrations of surface-exposed bond sites ($x_{M,\sigma}$), and chain ends ($x_{L,\sigma}$). $\Gamma_{N,\sigma}\,dt$, $\Gamma_{X,\sigma}\,dt$, and $\Gamma_{Y,\sigma}\,dt$ denote the probabilities of a site of type N, X, and Y, respectively, to be cut during infinitesimal dt, by any enzyme capable of attacking this site type, for sites exposed on class σ "smallest accessible compartment" (SAC) surfaces. They thus provide a much more direct indication, compared to the enzyme cutting rate coefficients, of how fast the hydrolysis process will take place. For the purpose of order-of-magnitude estimates, we treat Γ_N, Γ_X, and Γ_Y as time-independent and set each to its initial value at the start of hydrolysis ($t = t^{(o)} = 0$), from Eq. (22) in SI Section A of II.

Results and Discussion

Depolymerization Time of Decoupled Cellulose Chains

We will first discuss the time scales for hydrolyzing isolated chains by different types of enzymes and enzyme mixtures in the absence of solid/morphology effects. Thus, $x_M = x_V$. The geometry class index σ is therefore dropped from our notation in this section.

Pure Endo- and Pure Exo-Acting Enzymes

The single-chain hydrolysis times to depolymerize from an initial chain length $\ell = \mathrm{DP}^{(o)}$ to an average terminal length scale ℓ' can be estimated from simple "scaling arguments," as discussed in SI Section A for pure *endo*-acting enzyme systems, by

$$\tau^{(n)} \equiv \tau^{(n)}\left(\ell = \mathrm{DP}^{(o)} | \ell' = \frac{\ell_S}{2}\right) \sim \frac{2}{\Gamma_N \ell_S} \tag{1}$$

and, as discussed in SI Section B for pure *exo*-acting enzyme systems, by

$$\begin{aligned}\tau^{(x)} &\equiv \tau^{(x)}(\ell = \mathrm{DP}^{(o)} | \ell' = k_X) \sim \frac{\mathrm{DP}^{(o)} - k_X}{k_X\Gamma_X + k_Y\Gamma_Y} \\ &\equiv (\mathrm{DP}^{(o)} - k_X)\tau^{(1x)}\end{aligned} \tag{2}$$

From the depolymerization time-scale arguments in SI Section A, it is easy to see that pure *endo* fragmentation

Table I. Depolymerization time-scale estimates $\tau^{(n)}$ and conversion time simulation results $t(\ldots\text{–conv})$ (in units of 10^4 min) for the SS model and 50%, 90%, and 99% conversion, with pure *endo*-acting enzyme, $[EG1]^{(o)}$ from E1 enzyme system, and simulations for delta-function, Gaussian, and GP chain length distributions.

	$DP^{(o)} = 100$	$DP^{(o)} = 400$	$DP^{(o)} = 2{,}000$
Delta, t(0.50–conv)	0.78	0.81	0.82
Delta, t(0.90–conv)	1.13	1.16	1.17
Delta, t(0.99–conv)	1.20	1.23	1.24
Gauss, t(0.50–conv)	0.78	0.81	0.82
Gauss, t(0.90–conv)	1.13	1.16	1.17
Gauss, t(0.99–conv)	1.20	1.23	1.24
GP, t(0.50–conv)	0.78	0.81	0.83
GP, t(0.90–conv)	1.12	1.16	1.18
GP, t(0.99–conv)	1.20	1.23	1.25
$\tau^{(n)}$ $(DP^{(o)}\|3.5)$	1.22	1.23	1.23

Table II. Depolymerization time-scale estimates $\tau^{(x)}$ and conversion time simulation results $t(\ldots\text{–conv})$ (in units of 10^4 min) for the SS model and 50%, 90%, and 99% conversion, with pure *exo*-acting enzyme combination, $[CBH1,2]^{(o)}$ from E1 ensyme system, and simulations for delta-function, Gaussian, and GP chain length distributions.

	$DP^{(o)} = 100$	$DP^{(o)} = 400$	$DP^{(o)} = 2{,}000$
Delta, t(0.50–conv)	0.93	1.68	5.85
Delta, t(0.90–conv)	1.60	3.03	10.53
Delta, t(0.99–conv)	1.80	3.44	11.74
Gauss, t(0.50–conv)	0.90	1.69	5.86
Gauss, t(0.90–conv)	1.63	3.17	11.20
Gauss, t(0.99–conv)	1.90	3.92	11.43
GP, t(0.50–conv)	0.93	1.97	7.41
GP, t(0.90–conv)	2.10	5.38	22.59
GP, t(0.99–conv)	2.94	8.87	40.76
$\tau^{(x)}$ $(DP^{(o)}\|2)$	1.70	3.32	11.67

kinetics is essentially independent not only of the initial chain-length distribution shape but also of $DP^{(o)}$. This is also demonstrated by the numerical results in Table I, for several chain length distribution shapes, defined in Eqs. (35)–(37) of II, SI Section B. Note that indeed the 50% or 90% conversion times change by <2% when $DP^{(o)}$ is increased from 400 to 2,000, and by <1% if the initial distribution shape is changed from delta-function to Gaussian to Global Poisson (GP). Evidently, in the LCL, neither the initial DP nor the initial distribution shape matters. These time-scale estimation results thus provide a simple explanation for the simulation results shown in Figure 1 of II. The estimates of $\tau^{(n)}(DP^{(o)}|\ell' = \ell_S/2)$ are also quantitatively in good agreement with the 99% conversion time results obtained from full five-site model numerical simulations, as shown in Table I.

By contrast, in a pure *exo*-acting enzyme system, the depolymerization time is sensitive to both the average initial chain length, $DP^{(o)}$, and to the shape of the initial chain length distribution. In the case of the Gaussian and delta-function initial chain length distributions, most chains have about (or exactly) the same initial length $\ell \sim DP^{(o)}$ and they all complete their "race to depolymerization" in about the same amount of time. On the other hand, in the case of a GP distribution of the same $DP^{(o)}$, some chains are initially already much shorter than the average ℓ ($\sim DP^{(o)}$), and just as many are much longer. As a consequence of the linear ℓ-dependence of $\tau^{(x)}(\ell|\ell')$, these long chains with $\ell > DP^{(o)}$ are the "late runners in the race" (i.e., the runners with the longest distance to go); and the latest runners determine the overall duration of the race. Hence, the time to achieve, say, 90% hydrolytic conversion, for the same $DP^{(o)}$, is significantly longer for the Poisson than for the Gaussian or delta-function initial distributions, as seen in Table II. For the same reason, the 90% conversion time for the same distribution shape varies noticeably with $DP^{(o)}$: it increases about fourfold between $DP^{(o)} = 400$ and $DP^{(o)} = 2{,}000$, roughly consistent with the linear ℓ-dependence of $\tau^{(x)}(\ell|\ell')$. The estimated values of $\tau^{(x)}(DP^{(o)}|\ell' = k_X)$ are again in good agreement with the 99%-conversion time results from the full five-site model simulations for delta-function and Gaussian chains length distributions, as seen in Table II.

Mixed Endo–Exo-Acting Enzyme Systems

The foregoing order-of-magnitude depolymerization time can also be applied to gain a qualitative understanding of the competition (and cooperation) between *endo*- and *exo*-acting enzymes in a mixed enzyme system. Specifically, we can develop a "cross-over" criterion for the conditions under which a mixed *endo–exo* system will cross-over from *endo*-dominated to *exo*-dominated behavior. There are then three parameter regions, defined in terms of the relative magnitudes of the full *endo*-depolymerization time, $\tau^{(n)}(DP^{(o)}|\ell' = \ell_S/2)$, the full *exo*-depolymerization time, $\tau^{(x)}(DP^{(o)}|\ell' = k_X)$, and the single *exo*-cut time scale $\tau^{(1x)}$:

$$\text{Region I}: \quad \tau^{(1x)} > \tau^{(n)}; \quad \text{hydrolytic completion time} \sim \tau^{(n)} \tag{3}$$

$$\text{Region II}: \quad \tau^{(x)} > \tau^{(n)} \gg \tau^{(1x)}; \quad \text{hydrolytic completion time} \sim \tau^{(nx)} \tag{4}$$

$$\text{Region III}: \quad \tau^{(n)} \gg \tau^{(x)}; \quad \text{hydrolytic completion time} \sim \tau^{(x)} \tag{5}$$

where

$$\tau^{(nx)} \sim \frac{2}{[\Gamma_N(k_X\Gamma_X + k_Y\Gamma_Y)]^{1/2}} \tag{6}$$

In Region I (III), the "*endo*-limit" ("*exo*-limit"), the entire hydrolytic conversion proceeds essentially as in a pure *endo*-system (*exo*-system). In the intermediate Region II, however, *exo*-contribution to depolymerization is initially small but will gradually increase and finally dominate the

hydrolysis. Thus, we can define a characteristic "cross-over" chain length ℓ_{nx} when the *exo*-cutting rate matches the *endo*-cutting rate, from which $\tau^{(nx)}$ is then constructed, as shown in SI Section C.

In Table III, we summarize time-scale and cross-over length estimates, and the simulation results for different mixed enzyme systems, with delta-function initial chain-length distribution. The E1 mixed enzyme system is in the intermediate Region II. The time-scale estimates $\tau^{(nx)}$ are in order-of-magnitude agreement with the simulation results for the 99%-conversion times ~6,000 min. With the other enzyme systems in Table III, the parameter region changes from Region III to II to I, as the ratio between *endo*- and *exo*-enzyme concentrations, and $DP^{(o)}$ changes. The cross-over length decreases as $DP^{(o)}$ increases or as the *endo*/*exo*-enzyme concentration ratio decreases. This can be easily understood: increasing $DP^{(o)}$ reduces the initial concentration of chain ends. Thus, it takes longer for *endo*-enzymes to produce enough new chains ends for the *exo*-enzymes to attack, which leads to a larger ℓ_{nx}. The same reasoning applies when the relative concentration of *endo*-enzyme is decreased.

Synergy of *Endo–Exo*-Acting Enzyme Mixtures

In neither Region I nor III of the mixed enzyme systems will there be any significant synergy between *endo*- and *exo*-activity (Zhang and Lynd, 2006), since either one or the other is completely negligible in terms of producing new chain ends and/or soluble chain fragments. In Region II, the cooperative *endo–exo* hydrolysis kinetics is dominated by *endo*-activity during the initial stage, until the average chain length has been reduced to ℓ_{nx}; during the final stage thereafter, the kinetics is dominated by *exo*-activity. One important feature of this two-stage kinetics is the fact that during either stage the dominant, that is, the fastest, of the two enzymatic activities determines the duration of that stage, since both enzyme activities are of course working "in parallel" during either stage. Hence, the total cooperative hydrolysis time $\tau^{(nx)}$ can be significantly *less* than the hydrolysis times one would obtain with either pure *endo*- or pure *exo*-hydrolysis acting in isolation. This, in essence, is the origin of the hydrolysis "synergy."

As derived in SI Section D, the degree of synergy (DS) can be roughly estimated by

$$DS = \frac{1/\tau^{(nx)}}{1/\tau^{(n)} + 1/\tau^{(x)}} \tag{7}$$

From Table IV, we can see that the estimated DS, for a given enzyme mixture, is in good agreement with the simulation result for the maximum DS that can be attained by this enzyme system along the hydrolytic conversion up to near-completion. The five-site model numerical simulation results of DS(t) are based on the original definition, Eq. (18) in SI Section D. The time-scale-estimated (TSE) results from Table IV are also consistent with experimentally observed maximum DS values between 1.7 and 3.5 for Avicel substrates, using cellulases from *Trichoderma* species (Baker et al., 1998; Beldman et al., 1988; Hoshino et al., 1997; Kim et al., 1992; Medve et al., 1998; Woodward et al., 1988a). A detailed comparison with real experimental reports is provided in a later section.

Cellulose Hydrolysis in Solid Substrates: Initial Outermost Layer

The foregoing time-scale analysis of decoupled cellulose chains should be applicable in describing the short-time chain fragmentation kinetics at the initially enzyme-accessible outermost SAC layer, for any morphological model of the solid substrate, since there is no obstruction of access to the outermost layer. In Table V, we have estimated the initial outermost layer depolymerization times, and compared to numerical simulations, for the MS morphology model, defined in II. The simulation result, t(outer), is defined as the time to complete the initial solubilization of a fraction $x_M^{(o)} = \overline{F}_a^{(o)} x_V^{(o)}$ of the initial total solid monomer

Table III. Depolymerization time-scale estimates $\tau^{(\ldots)}$ (TSE) and conversion time simulation results $t(\ldots\text{–conv})$ (in units of 10^4 min) for the SS model with mixed enzymes, using original (A) and variants of (B and C) E1 enzyme concentrations, and simulation for delta-function initial chain length distribution.

	$DP^{(o)} = 100$	$DP^{(o)} = 400$	$DP^{(o)} = 2{,}000$
(A) $[EG1]^{(o)}$, $[CBH1,2]^{(o)}$			
t(0.99–conv)	0.61	0.63	0.64
TSE	$\tau^{(nx)} = 0.56$	$\tau^{(nx)} = 0.38$	$\tau^{(nx)} = 0.32$
ℓ_{nx}	15.4	22.6	27.1
Region	II	II	II
(B) 1% $[EG1]^{(o)}$, $[CBH1,2]^{(o)}$			
t(0.99–conv)	1.75	2.92	3.65
TSE	$\tau^{(x)} = 1.70$	$\tau^{(x)} = 3.32/\tau^{(nx)} = 3.81$	$\tau^{(nx)} = 3.18$
ℓ_{nx}	153.6	225.9	271.3
Region	III	III/II	II
(C) $[EG1]^{(o)}$, 1% $[CBH1,2]^{(o)}$			
t(0.99–conv)	1.19	1.21	1.24
TSE	$\tau^{(n)} = 1.21$	$\tau^{(n)} = 1.22$	$\tau^{(n)} = 1.23$
ℓ_{nx}	4.8	7.1	8.6
Region	I	I	I

Table IV. Degree of synergy DS from time-scale estimates (DS_{TSE}) [SI Eq. 7] and from simulation results, DS(t) at $t = 3{,}000$ min and at time of maximal *DS*, $t_{DS\text{-}max}$, [SI Eq. 18], for the SS model, with simulation for delta-function initial chain length distribution, $DP^{(o)} = 300$, using original and variants of the E1 enzyme concentrations.

	$[EG1]^{(o)}$, $[CBH1,2]^{(o)}$	50% $[EG1]^{(o)}$, $[CBH1,2]^{(o)}$	$[EG1]^{(o)}$, 50% $[CBH1,2]^{(o)}$
DS_{TSE}	2.36	2.63	1.92
DS (3,000 min)	1.86	1.97	1.57
DS ($t_{DS\text{-}max}$)	1.96	2.26	1.60
$t_{DS\text{–}max}$	6,000 min	8,520 min	7,800 min

Table V. Initial outermost layer depolymerization time simulation results t(outer) (estimated from early arrest in rise of $|dx_V/dt|$) for MS/MM model, and time-scale estimates (TSE) $\tau^{(\cdots)}$ (in units of 10^2 min), with simulation for delta-function initial chain length distribution, $DP^{(o)} = 300$, $\overline{F}_a^{(o)} = 0.006$, using original and variants of E1 enzyme concentrations.

	$[EG1]^{(o)}$, $[CBH1,2]^{(o)}$	1% $[EG1]^{(o)}$, $[CBH1,2]^{(o)}$	10% $[EG1]^{(o)}$, $[CBH1,2]^{(o)}$	$[EG1]^{(o)}$, 10% $[CBH1,2]^{(o)}$	$[EG1]^{(o)}$, 1% $[CBH1,2]^{(o)}$
t(outer)	1.76	25.02	7.69	1.90	1.94
TSE	$\tau^{(n)} = 1.39$	$\tau^{(nx)} = 31.92$	$\tau^{(nx)} = 10.14$	$\tau^{(n)} = 1.39$	$\tau^{(n)} = 1.39$
ℓ_{nx}	3.1	30.5	9.6	0.9	0.3
Region	I	II	II	I	I

concentration $x_V^{(o)}$. This is also in close agreement with the time of arrest in the initial rise of $|dx_V/dt|$, as shown for both MS and MM models in II. For the E1 system, the MS model is *endo*-limited (Region I) and its estimated *endo*-depolymerization time is $\tau^{(n)} \sim 139$ min, which agrees with, and explains, the very short initial depolymerization time in the MS model simulation, t(outer) ~ 180 min. Table V also shows that the time-scale estimates for a wide range of enzyme concentrations are quite consistent with the MS model simulation results for the outermost layer depolymerization times. We have also verified that, consistent with II, MS and MM models will give rise to the same outermost layer depolymerization time, for identical enzyme parameters and initial values $\overline{F}_a^{(o)}$, $x_V^{(o)}$, and $DP^{(o)}$.

Quasi-Steady-State Approximation for Long Time Scales

A crucial feature of the morphology-based surface ablation models (MS and MM) is the fact that the overall hydrolytic conversion time scale, denoted by $\tau^{(s)}$ below, can be orders of magnitude longer than the initial outermost layer depolymerization time scale ($\tau^{(n)}$ or $\tau^{(nx)}$). The latter, as discussed, is adequately described by the non-morphological isolated chain picture. However, to understand the much longer hydrolysis time scale $\tau^{(s)}$, we have to take into account the effects of steric obstruction in the solid substrate morphology. As described in detail in SI Section E, the order-of-magnitude separation of time scales, $\tau^{(s)} \gg \tau^{(n)}$, $\tau^{(nx)}$, can be exploited by treating the long-time behavior in a quasi-steady-state (QSS) approximation.

One important QSS result is a simple approximate relation between relative hydrolysis rate $\Gamma_{rel} \equiv (1/x_V)|dx_V/dt|$, and (geometry-averaged) accessibility fraction $\overline{F}_a$:

$$\Gamma_{rel} \cong \frac{1}{\tau^{(\lambda)}} \overline{F}_a \tag{8}$$

which holds regardless of morphology details. Here $\tau^{(\lambda)}$ is an effective "single-layer ablation time" scale, which is of the same order as $\tau^{(n)}$ and given by Eq. (27) of SI Section E.

This result is easy to understand. The ablation process happens at the SAC surfaces and, all other things being equal, its total rate must be proportional to the total surface area. Hence, its *relative* hydrolysis rate must be proportional to the *relative* surface area which is, by definition, $\overline{F}_a$. This provides a simple explanation for the close correlation between Γ_{rel} and $\overline{F}_a$, as demonstrated already in the simulation results Figure 3C and D of II: the Γ_{rel}-curves in Figure 3C should track $\overline{F}_a$ in Figure 3D, with an approximately constant ratio $\Gamma_{rel}/\overline{F}_a = 1/\tau^{(\lambda)}$ that is independent of time and independent of the underlying shape of the SAC size morphology distribution $\Xi(\lambda_\sigma^{(o)})$. This is of course only approximately obeyed by the full model simulation results, due to the approximations in the QSS approach and due to the neglect of the (weak) time-dependence of $\tau^{(\lambda)}$. However, the general trends in the simulation results are correctly reproduced by Eq. (8).

QSS Time-Scale Analysis for the MS Model

Applying the general QSS solution in SI Section E to the MS model (with index $\sigma = 1 \equiv M_{MD}$ suppressed here), we can solve SI Eq. (28) for the hydrolytic conversion time $\tau^{(s)}$ where a fraction $1 - \varepsilon$ of the substrate has been solubilized:

$$\tau^{(s)} \cong \tau^{(\lambda)} \lambda^{(o)} (1 - \varepsilon^{1/d_A}) \cong \tau^{(\lambda)} \frac{d_A (1 - \varepsilon^{1/d_A})}{\overline{F}_a^{(o)}} \tag{9}$$

here, $\lambda^{(o)} \cong d_A/\overline{F}_a^{(o)}$ and $\overline{F}_a^{(o)}$ denotes the initial accessibility fraction. Using $\overline{F}_a^{(o)} = 0.006$ and $d_A = 2$, we get $\tau^{(s)} \sim 12,100$ min for 50% conversion ($\varepsilon = 0.5$) and $\tau^{(s)} \sim 37,100$ min for 99% conversion ($\varepsilon = 0.01$). This agrees quite well with the 50% and 99% conversion times of 10,700 and 28,000 min, respectively, obtained from the full MS model simulation, as shown in Table VI. From the table, one can see that the time-scale estimations agree with the simulations over a wide range of enzyme concentrations. Quantitatively, Eq. (9) is likely an overestimate of the hydrolysis time because it neglects the fact that Γ_N, Γ_X, and Γ_Y are (weakly) increasing with time during hydrolysis.

If we compare the overall hydrolysis time-scale $\tau^{(s)}$ to the MS model chain depolymerization time, estimated, for example, by $\tau^{(n)}$, we get from Eqs. (1) and (9) for $\varepsilon \to 0$:

$$\frac{\tau^{(s)}}{\tau^{(n)}} \sim \frac{d_A}{\overline{F}_a^{(o)}} \cong \lambda^{(o)} \tag{10}$$

Table VI. Conversion time-scale estimates $\tau^{(s)}$ and simulation results $t(\ldots\text{–conv})$ (in units of 10^4 min) for 50% and 99% conversion in the MS model, with simulation for delta-function initial chain length distribution, $DP^{(o)} = 300$, $\overline{F}_a^{(o)} = 0.006$, using original and variants of E1 enzyme concentrations.

	$[EG1]^{(o)}$, $[CBH1,2]^{(o)}$	10% $[EG1]^{(o)}$, $[CBH1,2]^{(o)}$	$[EG1]^{(o)}$, 10% $[CBH1,2]^{(o)}$	$[EG1]^{(o)}$, 1% $[CBH1,2]^{(o)}$
t(0.50–conv)	1.07	5.33	1.27	1.30
$\tau^{(s)}$ (0.50–conv)	1.21	4.58	1.44	1.47
t(0.99–conv)	2.80	14.50	3.27	3.33
$\tau^{(s)}$ (0.99–conv)	3.71	14.08	4.43	4.50
$\tau^{(\lambda)}$	0.012	0.047	0.015	0.015

since $\tau^{(\lambda)}$ and $\tau^{(n)}$ are of the same order of magnitude, that is, $\tau^{(\lambda)}/\tau^{(n)} \sim \mathcal{O}(1)$, by Eqs. (1) and (27). This makes it explicit that the order-of-magnitude separation of the two fundamental time scales in surface layer ablation models is primarily controlled by just one single substrate parameter: the accessibility fraction $\overline{F}_a^{(o)}$, or equivalently, by the number of layers $\lambda^{(o)}$ per SAC. Given that $\overline{F}_a^{(o)}$ typically never exceeds values of 10%, even in the "most accessible" substrate materials (Zhang and Lynd, 2004), we must conclude that in most cellulosic substrates, $\tau^{(s)}$ and $\tau^{(n)}$ are separated by at least one order of magnitude, regardless of the precise values of the enzymatic kinetics parameters. Crucially, by Eq. (9), it is *both* substrate morphology, via $\lambda^{(o)}$, and enzyme kinetics, via $\tau^{(\lambda)}$, which jointly determine the hydrolytic conversion time.

QSS Time-Scale Analysis and Hydrolysis Slow Down in MM Models

Hydrolysis slow down is commonly observed in enzymatic conversion of solid cellulose, often after very short conversion times (Yang et al., 2006; Zhang et al., 1999). However, as noted in II and explained by the QSS analysis in SI Section F, the relative hydrolysis rate $\Gamma_{rel}(t)$ always *increases* during hydrolysis in the MS model where all SACs are assumed to be of the same size $\lambda(t)$. A significant hydrolysis slow down, with decreasing $\Gamma_{rel}(t)$, can only be observed in MM models with very broad SAC size morphology distributions.

To investigate this further within the QSS framework, we consider here first the simplest possible MM model: a bi-modal morphology distribution, comprising only two distinct SAC sizes, that is, $\sigma = 1, 2 \equiv M_{MD}$. While "two-substrate models" have previously been invoked on phenomenological grounds to explain the hydrolysis slow down (Gonzalez et al., 1989; Nidetzky and Steiner, 1993; Scheiding et al., 1984), the bi-modal model provides an explicit realization of the "two substrates" in terms of a mesoscopic characterization of substrate morphology. As shown in SI Section F, SI Figure 1, hydrolysis slow-down behavior is found in this model if we assume sufficiently disparate initial SAC sizes, $\lambda_1^{(o)} \ll \lambda_2^{(o)}$, with comparable initial molar monomer contents, $x_{V,1}^{(o)}$ and $x_{V,2}^{(o)}$, for the two SAC types $\sigma = 1, 2$. (This is also verified by solving the full surface layer ablation model without QSS for the bi-modal distribution.) It can also be easily seen that the SAC size morphology distributions will substantially affect the time scale over which Γ_{rel} exhibits decline and consequently the extent of the hydrolysis slow down. Qualitatively, the same behavior can be found for MM models with, for example, a uniform continuous initial SAC size distribution, over some $\lambda_\sigma^{(o)}$-range from $\Lambda_0^{(o)}$ and $\Lambda_1^{(o)}$. For $\Lambda_0^{(o)} \ll \Lambda_1^{(o)}$ the MM model does indeed exhibit hydrolysis slow down: an initial decline, followed by a minimum, in $\Gamma_{rel}(t)$. On the other hand, for $\Lambda_0^{(o)} \to \Lambda_1^{(o)}$, or for a narrow Gaussian initial SAC size distribution, the morphology distribution approaches a delta-function, that is, an MS model; the hydrolysis slow down is suppressed; and $\Gamma_{rel}(t)$ rises monotonically, as in the MS model. This is illustrated by the results in SI Figure 2, discussed further in SI Section G. The foregoing comparative MM model results further support the notion that hydrolysis slow down may be partially attributed to substrate morphology heterogeneity, that is, to a sufficiently wide SAC size morphology distribution, as proposed in II.

General QSS results for the MM model kinetics are given in SI Section G, using either Eqs. (30) and (31) or Eqs. (38) and (39). For the special case of the uniform distribution model, an analytic solution can be achieved and is provided. For a fast and effective estimation of general MM model time scales, we can replace the MM model by a corresponding MS model, using Eq. (9) with a $\lambda^{(o)}(MS)$ equal to the mean $\lambda_\sigma^{(o)}$, weighted with the MM model morphology distribution $\Xi(\lambda_\sigma^{(o)})/M_\Xi$, as defined in SI Section E. In Table VII, such approximate MS-based time-scale estimates are compared to full MM model simulation results for uniform and Gaussian SAC size morphology distributions. For the MM model with uniform SAC size morphology distribution, its approximating MS model has $\lambda^{(o)}(MS) = 830$ and $\overline{F}_a^{(o)}(MS) = 0.0024$; and for the Gaussian SAC size morphology distribution, $\lambda^{(o)}(MS) = 458$ and $\overline{F}_a^{(o)}(MS) = 0.0044$; whereas $\overline{F}_a^{(o)}(MM) = 0.006$ in both MM models. The MS $\tau^{(s)}$-results in Table VII agree very well with the MM simulation results for a wide range of enzyme concentrations. Hence, Eq. (9) is more generally valid, even for MM models, if $\lambda^{(o)}$ is replaced by an appropriately weighted mean of the initial SAC sizes $\lambda_\sigma^{(o)}$.

Table VII. Conversion time-scale QSS estimates $\tau^{(s)}$ and simulation results $t(\ldots\text{–conv})$ (in units of 10^4 min) for 50% and 99% conversion.

	$[EG1]^{(o)}$, $[CBH1,2]^{(o)}$	10% $[EG1]^{(o)}$, $[CBH1,2]^{(o)}$	$[EG1]^{(o)}$, 10% $[CBH1,2]^{(o)}$	$[EG1]^{(o)}$, 1% $[CBH1,2]^{(o)}$
(A) MM82-1 uniform morphology (SAC size) distribution				
t(0.50–conv)	1.62	8.57	1.89	1.92
$\tau^{(s)}$ (0.50–conv)	2.18	9.97	2.48	2.51
t(0.99–conv)	8.29	46.01	9.37	9.50
$\tau^{(s)}$(0.99–conv)	6.72	30.64	7.63	7.74
$\tau^{(\lambda)}$	0.009	0.041	0.011	0.011
(B) MM82-2 Gaussian morphology (SAC size) distribution				
t(0.50–conv)	1.20	6.08	1.42	1.46
$\tau^{(s)}$(0.50–conv)	1.46	5.98	1.70	1.73
t(0.99–conv)	4.57	24.60	5.25	5.33
$\tau^{(s)}$(0.99–conv)	4.48	18.38	5.24	5.33
$\tau^{(\lambda)}$	0.011	0.044	0.013	0.013

Simulations are for MM model with uniform (A) or Gaussian (B) SAC size distribution $\Xi(\lambda)$, delta-function initial chain length distribution, $DP^{(o)} = 300$, $\overline{F}_a^{(o)} = 0.006$, using original and variants of E1 enzyme concentrations. Time-scale estimates are for MS model with same parameters as corresponding MM model, but with $\lambda^{(o)}$(MS) set to MM model mean of $\lambda_\sigma^{(o)}$, weighted with $\Xi(\lambda_\sigma^{(o)})/M_\Xi$ (see context for details).

Comparisons With Experiments

In this section, we compare our time-scale analysis for conversion times and DS with real experimental data from the literature. Our cellulose hydrolysis model parameters (in Table I of II) were originally extracted (Zhang and Lynd, 2006) from experiments by Beldman et al. (1987), Steiner et al. (1988), and Tomme et al. (1988). For a meaningful comparison, we have thus selected experiments that measured conversion time and DS under experimental settings, and in particular with enzymatic parameters, that are similar to the foregoing "parameterization" experiments. The selected experiments, included in Figure 1 and Table VIII, used cell-free cellulases (i.e., endoglucanases and exoglucanases) from *T. reesei* (or *Trichoderma viride*), either naturally mixed or purified using protein assays, to hydrolyze model microcrystalline cellulose Avicel in 50 mM sodium acetate buffer (pH 4.8) at 50°C, unless stated otherwise. If a cellulase enzyme mixture was used in the experiment, we assumed typical weight fractions of 0.6, 0.2, and 0.12 for CBH1, CBH2, and EG1, respectively. Commonly used Avicel models include Avicel PH105, PH101, and PH102. Despite their major difference in the average particle size, that is, 20, 50, and 100 μm, respectively, their cellulose content, DP, crystallinity index, enzyme adsorption, and surface accessible area are almost same (Sangseethong et al., 1998). Although there are some differences in their performance of hydrolysis (Fig. 1 of Sangseethong et al., 1998), we treat them as the same and use $DP = 300$ and $\overline{F}_a = 0.006$ to represent their characteristics. Since we do not know the SAC distributions within these real cellulosic substrates, we compare to conversion time-scale estimates using both the Gaussian (narrow) and the uniform (wide) SAC distributions described in II.

Conversion Time-Scale Estimates for Experiments in Yang et al. (2006)

Avicel PH101 20 g/L (Sigma, St. Louis, MO) and *T. reesei* cellulase system Spezyme CP 4.1 g/L (60 FPU/g cellulose; Genencor, Palo Alto, CA) were used in 40 mL solution. Hydrolysis conversion experimental results are extracted from Table I of the article. As shown in Figure 1A, conversion time-scale estimates from both Gaussian and uniform SAC distributions are in good agreement with the experiments in the short hydrolysis phase (i.e., <4 h).The large discrepancy between estimates and experimental data at longer times (i.e., 15 h) may be caused by the fact that the study did not use β-glucosidases which hydrolyze soluble oligomer sugars (such as cellobiose, a well-known inhibitor of cellulase enzymes) into glucose, thus reduce the inhibitory factor, while in our current modeling and estimation, the product inhibition is ignored.

Conversion Time-Scale Estimates for Experiments in Hong et al. (2007)

Avicel PH105 10 g/L (FMC Corp., Philadephia, PA) and cellulase Spezyme CP 0.51 g/L (15 FPU cellulase/g Avicel; Genencor, Palo Alto), together with 30 IU cellobiase/g Avicel, were used in 400 mL of 50 mM citrate buffer (pH 4.8) at 50°C. Hydrolysis conversion experimental results are extracted from Figure 4 of the article. The differences between estimates and experiment at long times, as shown in Figure 1B, are much less than those in Figure 1A, likely because β-glucosidases were used in this study.

Conversion Time-Scale Estimates for Experiments in Bommarius et al. (2008)

Avicel PH101 100 g/L (Fluka, St. Louis, MO) and cellulase 0.27 g/L (1.5 U/8 mL) from *T. reesei* ATCC 26921 (Celluclasts C2730; Sigma), together with 30 U/8 mL β-glucosidase from almonds (G0395; Sigma), were used in 8 mL of 50 mM sodium acetate buffer (pH 5.0) at 50°C. Hydrolysis conversion experimental results are extracted from Figure 11 of the article and compared to our estimates in Figure 1C. In this study, the authors actually first tested the amount of β-glucosidase needed to maximally reduce

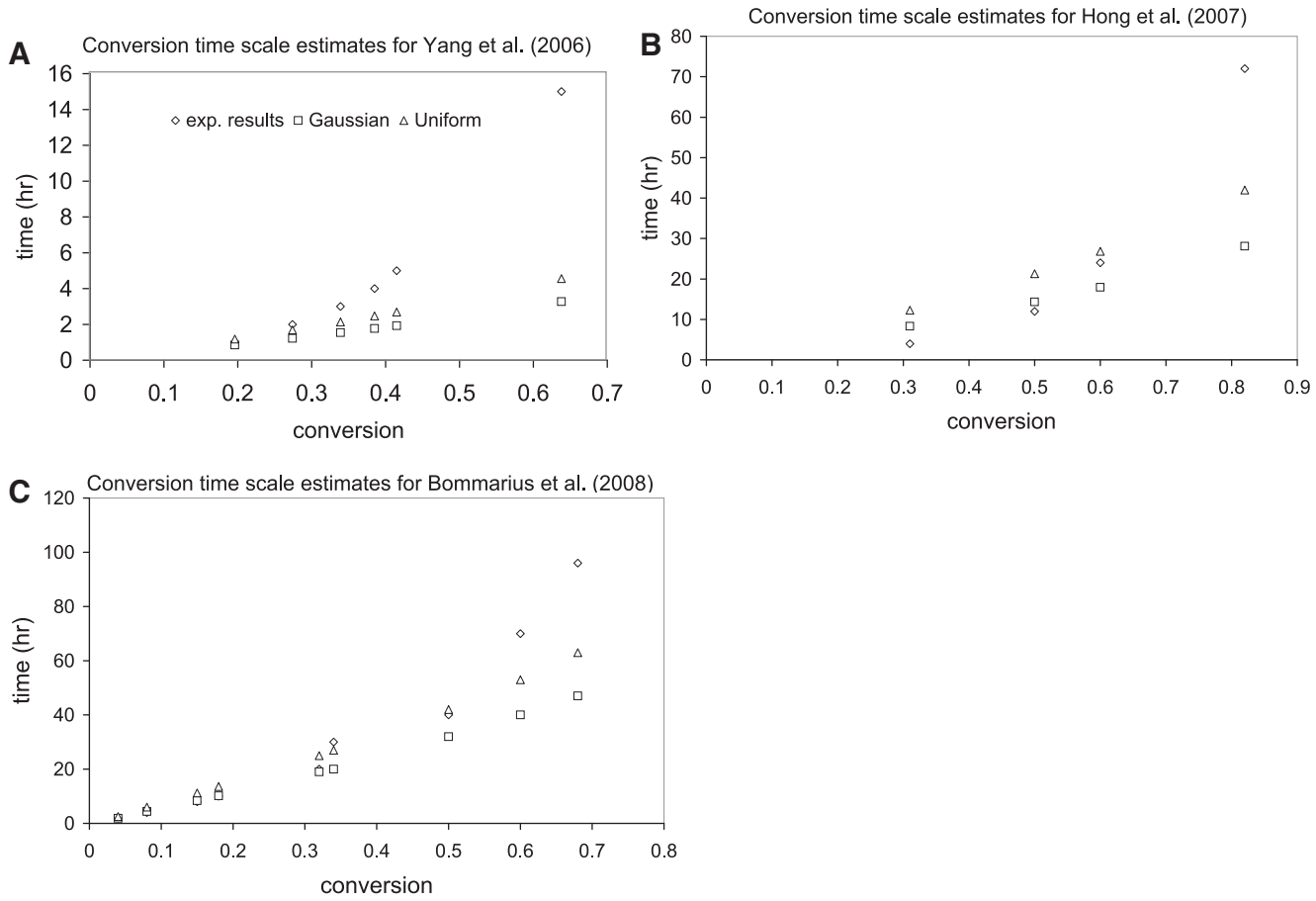

Figure 1. Estimates of conversion time-scale ($\tau^{(s)}$) for real experiments in Yang et al. (2006), Hong et al. (2007), and Bommarius et al. (2008). ◇ represents the experimental results (averages if there are replicates). □ represents the estimates of conversion time scale using the Gaussian SAC distribution. ■ represents the estimates of conversion time scale using the Uniform SAC distribution.

Table VIII. Estimates of DS (DS_{TSE}) for real experiments in Kim et al. (1994), Medve et al. (1998), and Woodward et al. (1988b).

Kim et al. (1994)							
EndoI:ExoII	2:1	1:1	1:2				
Exp. results	1.33	1.48	1.46				
DS_{TSE}	1	1.34	1.74				
EndoII:ExoII	2:1	1:1	1:2				
Exp. results	1.47	1.49	1.34				
DS_{TSE}	0.7	1.1	1.34				
Medve et al. (1998)							
CBHI:EGII	1:1						
Exp. results	1.43						
DS_{TSE}	1.34						
Woodward et al. (1988b)							
EGII, CBHI, II	120, 75, 75 μg/mL			64, 40, 40		5, 10, 5	
Exp. results	1.2			1.37		2.03	
DS_{TSE}	1.31			1.35		1.86	
CBHI = 140		EGII = 5	EGII = 10	EGII = 20	EGII = 40	EGII = 80	EGII = 140
Exp. results		1.28	1.2	1.42	1.18	1.1	0.92
DS_{TSE}		2.25	2.28	2.04	1.66	1.27	1

Details are given in the context.

the inhibition of soluble oligomers, mainly cellobiose. They found that the total activity of β-glucosidase in the reaction volume must be 20 times higher than that of cellulase (Fig. 5 of the article), which was then applied in all experiments. As expected, our conversion time-scale estimation performs the best with this experimental data set, showing good agreement up to 60% conversion (see Fig. 1C).

There are of course many other factors, besides product inhibition, that could slow down the cellulose hydrolysis, such as enzyme degradation, inactive binding, and jamming effects (Bommarius et al., 2008), which has not yet been taken into account in our modeling, and thus estimation. However, the general trends seen across Figure 1A–C strongly suggest that our time-scale estimation works well under the conditions for which it was constructed, that is, as long as the underlying enzyme system remains fully intact and operational, undegraded and uninhibited. As such, it is notable that the predictions and estimations of the current model are limited in capturing the full degree of hydrolysis rate slow down that has been observed in experiments. This limitation is due to the incomplete consideration of known hydrolysis slow down causes in our model and other possible unknown mechanisms that has not been discovered or well characterized. The full understanding of the hydrolysis slow down in a systematic way and solutions to diminish such effects in the cellulose hydrolysis process are certainly worth more research efforts.

DS Estimates for Experiments in Kim et al. (1994), Medve et al. (1998), and Woodward et al. (1988b)

Kim et al. (1994) used Avicel PH101 10 g/L (FMC Corp.) and Endo I, II, and Exo II, total 0.3 mg/mL, isolated from a commercial cellulase Meicelase TP60 from *Trichoderrna viride* with molecular weight 52K, 60K, and 62K, respectively, in 5 mL solution. The specific enzyme activity for Endo II is assumed here to be twice that of Endo I in our estimation, as suggested by the experimental data in this study. DS experimental results are extracted from Figure 5 of the article, where the experimental data were measured after 24 h hydrolysis. Medve et al. (1998) used Avicel M2331 10 g/L (Merck, Darmstadt, Germany) and CBH I and EG II, each 0.16 μmol/g Avicel, purified from a commercial cellulase Celluclast from *T. reesei* (Novo Nordisk, Bagsvaerd, Denmark) in 2 mL solution. DS experimental results are extracted from Figure 3 of the article, and the average DS over the time course of 50 h is used to represent the DS of the reaction system. Woodward et al. (1988b) used Avicel PH105 10 g/L (FMC Corp.) and CBH I, II, and EG II (μg/mL), purified from *T. reesei* (Genencor, San Francisco, CA), together with β-glucosidase from *Aspergillus niger* (Sigma), in 5 mL solution. DS experimental results are extracted from Figures 2 and 4 of the article, and the average DS over the time course of 7 h is used to represent the DS of the reaction system. As shown in Table VIII, our DS estimates are in reasonable agreement with, and reproduce the general trends with enzyme mixing ratios in, experimental results over a wide range of concentrations. Notably, however, in less endo-acting systems, the estimated DS values are systematically higher than in the experiments. This is probably due to the fact that again we did not consider such effects as enzyme deactivation/degradation. Thus, the enzymes in our model are at all times as fresh and active as new ones, whereas in the real experiments, they are not. As a result, the endo–exo synergy mainly caused, as suspected, by the promotion of cellulose-ends generation through endo-acting enzymes is more over-counted in our model prediction after the enzyme deactivation/degradation effects start taking place in less endo-acting systems. Inclusion of such model refinements will be the target of future work.

Conclusion

In conclusion, we have presented detailed time-scale analyses for the enzyme-catalyzed hydrolytic conversion of solid cellulosic substrates. These analyses are developed here within the context of both non-morphological and solid-morphology-based enzymatic chain fragmentation kinetics models. They cover free enzyme activity comprising both *endo*- and *exo*-acting components of, in principle, any compositional complexity.

The first one of these analyses applies specifically to non-morphological enzymatic chain cutting models (Okazaki and Moo-Young, 1978; Suga et al., 1975; Zhang and Lynd, 2006). These models treat individual chains effectively in isolation and do not account for the mutual steric obstruction arising in dense assemblies of chains embedded in a solid substrate. A central result from this non-morphological analysis is the identification of depolymerization time scales in three distinct kinetic parameter regimes, including *endo*- and *exo*-dominated regions; and an intervening intermediate region, characterized by highly cooperative, synergistic *endo–exo* chain fragmentation activity with a significant degree of synergy.

These non-morphological results are then integrated into the analysis of a more realistic fully morphological hydrolysis kinetics modeling framework which incorporates: enzymatic chain fragmentation; mutual steric obstruction; chain exposure by hydrolytic surface ablation; and, in turn, hydrolytic evolution of the underlying solid substrate morphology. This analysis explains not only the existence but also the quantitative magnitudes of two very distinct characteristic time scales that had been identified previously, in numerical simulations of morphology-controlled hydrolytic surface ablation kinetics, described in II. Specifically, the numerically observed early rapid rise and arrest in the hydrolysis rate can be identified with a very short "single-layer ablation time" $\tau^{(\lambda)}$ that is basically identical with the non-morphological depolymerization time scale. The much longer time scale $\tau^{(s)}$ for near-complete hydrolytic conversion of the entire substrate is then naturally explained by the way of a QSS analysis. The

QSS analysis shows that $\tau^{(s)}$ is essentially the product of a purely non-morphological enzymatic factor, the "single-layer ablation time" $\tau^{(\lambda)}$; and of a purely morphological factor, the number of such "ablation layers" $\lambda^{(o)}$ comprised in a typical smallest enzyme-accessible substrate compartment.

While explaining in mathematically simple and physically transparent terms the fundamental time scales in morphology-controlled hydrolytic surface ablation kinetics, the foregoing analyses also provide a potentially very useful *algebraic* estimation tool to relate engineering-relevant systems variables to basic enzyme kinetics and morphology parameters, without having to solve extensive systems of coupled kinetics ODEs. As demonstrated here by detailed comparisons to highly accurate numerical ODE solutions, our approximate time-scale analysis generate reasonable estimates, for example, for hydrolytic conversion times, to within 30% of the quasi-exact numerical values, or better; and they do so over a wide range of enzymatic and substrate parameters. The time-scale analyses therefore afford us with a fast, convenient semi-quantitative framework for the calculation of systems variables such as single-layer depolymerization and hydrolytic conversion times; macroscopic kinetics variables such as absolute and relative conversion rates; and hydrolytically evolving morphology variables such as SAC sizes and surface accessibility fractions. Our conversion time and degree of synergy estimates based on time-scale analysis are in reasonable agreement with observed magnitudes and general trends with enzyme mixing ratios, as seen in experimental data under experimental settings most closely matching our modeling assumptions. Future refinements will address effects currently not included in the model, such as enzyme degradation and product inhibition.

Nomenclature

$[\mathrm{CBH1}]^{(o)}$	CBH1 concentration in the "E1" enzyme system of II
$[\mathrm{CBH2}]^{(o)}$	CBH2 concentration in the "E1" enzyme system of II
$d_{A,\sigma}$	ablation dimension for class-σ SACs
$[\mathrm{EG1}]^{(o)}$	EG1 concentration in the "E1" enzyme system of II
$F_{a,\sigma}$	fraction of accessible G_1 for class-σ SACs ($\equiv n_{M,\sigma}/n_{V,\sigma}$)
$\overline{F}_a$	overall accessibility fraction of accessible G_1 ($\equiv n_M/n_V$)
k_X (k_Y)	site position from L-end (R-end) where exo-L (exo-R) act at
ℓ	number of G_1-monomers in an insoluble glucan chain G_ℓ
ℓ_{nx}	*endo–exo* "cross-over" chain length
ℓ_S	minimum insoluble chain length
$L_{\kappa,\mu}$	adsorption coefficient for (κ, μ) ES complex (1/mM)
M_{MD}	population size of SAC geometries
u_κ	total type-κ enzyme concentration (mM)
v_κ	free type-κ enzyme concentration (mM)
x_M	total concentration of G_1 exposed on surfaces (mM)
$x_{M,\sigma}$	concentration of G_1 exposed on class-σ SAC surfaces (mM)
x_v	total concentration of G_1 in solid substrate (mM)
$x_{V,\sigma}$	concentration of G_1 contained in class-σ SACs (mM)
$x_{\mu,\sigma}$	concentration of type-ν site exposed on class-σ SAC surfaces (mM, $\equiv C_\sigma n_{\nu,\sigma}$)
$y_{\mu,\sigma}$	concentration of free type-μ sites on class-σ SAC surfaces (mM)

Greek Symbols

$\gamma_{\kappa,\mu}$	cutting rate coefficient (cuts per time per (κ, μ) ES complex)
$\Gamma_{\mu,\sigma}$	enzyme cutting rate factors defined by Eqs. (19)–(21) of II SI
Γ_{rel}	relative hydrolysis rate ($\equiv -\mathrm{d}x_V/\mathrm{d}t/x_V$)
ε	fraction of unconverted solid substrate ($\equiv x_V(t)/x_V(t^{(o)})$)
κ	index of enzyme types, $\kappa = 1$, 2, or 3 represent the *endo-*, *exo-L-*, and *exo-R*-acting glucanase, respectively
λ_σ	layer number variable of class-σ SACs
$\Lambda_0^{(o)}$	minimum of from $\lambda_1^{(o)}$ to $\lambda_{M_{MD}}^{(o)}$
$\Lambda_1^{(o)}$	maximum of from $\lambda_1^{(o)}$ to $\lambda_{M_{MD}}^{(o)}$
ν, μ	index of site types, N, L, R, X, Y, Z, or o
$\Xi(\lambda)$	morphology distribution of initial SAC sizes $\lambda_\sigma^{(o)}$
σ	index of SAC classes
$\tau^{(n)}$	time-scale estimate for pure *endo*-acting enzyme system
$\tau^{(nx)}$	time-scale estimate for mixed *endo-exo*-acting enzyme system
$\tau^{(x)}$	time-scale estimate for pure *exo*-acting enzyme system
$\tau^{(1x)}$	time-scale estimate for a single *exo*-cut
$\tau^{(s)}$	time-scale estimate for $1-\varepsilon$ conversion of solid-morphology substrate
$\tau^{(\lambda)}$	effective single-layer ablation time-scale estimate
M_Ξ	$M_\Xi = \sum_{\sigma=1}^{M_{MD}} \Xi(\lambda_\sigma^{(o)})$

Abbreviations

I	companion article I, Zhou et al. (2009a)
II	companion article II, Zhou et al. (2009b)
DP	degree of polymerization
DS	degree of synergy
GP	global Poisson
LCL	long chain limit
MM	"*M*ultiple-layer, *M*ultiple-geometry" model
MM82-1	the MM model with uniform distribution of monomer concentration over SAC size, SI Section E, Eq. (32)
MM82-2	the MM model with Gaussian distribution of monomer concentration over SAC size, SI Section E, Eq. (33)
MS	"*M*ultiple-layer, *S*ingle-geometry" model
QSS	quasi-steady state
SAC	smallest accessible compartment
SS	"*S*ingle-layer, *S*ingle-geometry" model
TSE	time-scale estimate

We acknowledge the U.S. Department of Energy (grant # 4000063512) and the National Science Foundation (grant #: NSF/DBI-0354771, NSF/ITR-IIS-0407204, NSF/DBI-0542119, and NSF/CCF0621700) for financial support. We also acknowledge computing support from the University of Georgia Research Computing Center. The BioEnergy Science Center is supported by the Office of Biological and Environmental Research in the DOE Office of Science.

References

Baker JO, Ehrman CI, Adney WS, Thomas SR, Himmel ME. 1998. Hydrolysis of cellulose using ternary mixtures of purified cellulases. Appl Biochem Biotechnol 70/72:395–403.

Beldman G, Voragen AGJ, Rombouts FM, Searle-van Leeuwen MF, Pilnik W. 1987. Adsorption and kinetic behavior of purified endoglucanases

and exoglucanases from *Trichoderma viride*. Biotechnol Bioeng 30:251–257.

Beldman G, Voragen AGJ, Rombouts FM, Pilnik W. 1988. Synergism in cellulose hydrolysis by endoglucanases and exoglucanases purified from *Trichoderma viride*. Biotechnol Bioeng 31:173–178.

Bommarius AS, Katona A, Cheben SE, Patel AS, Ragauskas AJ, Knudson K, Pu Y. 2008. Cellulase kinetics as a function of cellulose pretreatment. Metab Eng 10:370–381.

Converse AO, Optekar JD. 1993. A synergistic kinetics model for enzymatic cellulose hydrolysis compared to degree-of-synergism experimental results. Biotechnol Bioeng 42:145–148.

Fenske JJ, Penner MH, Bolte JP. 1999. A simple individual-based model of insoluble polysaccharide hydrolysis: The potential for autosynergism with dual-activity glycosidases. J Theor Biol 199:113–118.

Gonzalez G, Caminal G, de Mas C, Lopez-Santin J. 1989. A kinetic model pretreated wheat straw saccharification by cellulose. J Chem Technol Biotechnol 44:275–288.

Goyal A, Ghosh B, Eveleigh D. 1991. Characteristics of fungal cellulases. Biores Technol 36:37–50.

Hong J, Ye X, Zhang YHP. 2007. Quantitative determination of cellulose accessibility to cellulase based on adsorption of a non-hydrolytic fusion protein containing CBM and GFP with its applications. Langmuir 23:12535–12540.

Hoshino E, Shiroishi M, Amano Y, Nomura M, Kanda T. 1997. Synergistic actions of exo-type cellulases in the hydrolysis of cellulose with different crystallinities. J Ferment Bioeng 84:300–306.

Kim DW, Kim TS, Jeong YK, Lee JK. 1992. Adsorption kinetics and behaviors of cellulase components on microcrystalline cellulose. J Ferment Bioeng 73:461–466.

Kim DW, Jeong YK, Lee JK. 1994. Adsorption kinetics of exoglucanase in combination with endoglucanase from *Trichoderma viride* on microcrystalline cellulose and its influence on synergistic degradation. Enzyme Microb Technol 16:649–658.

Medve J, Karlsson J, Lee D, Tjerneld F. 1998. Hydrolysis of microcrystalline cellulose by cellobiohydrolase I and endoglucanase II from *Trichoderma reesei*: Adsorption, sugar production pattern, and synergism of the enzymes. Biotechnol Bioeng 59:621–634.

Nidetzky B, Steiner W. 1993. A new approach for modeling cellulase cellulose adsorption and the kinetics of the enzymatic hydrolysis of microcrystalline cellulose. Biotechnol Bioeng 42:469–479.

Okazaki M, Moo-Young M. 1978. Kinetics of enzymatic hydrolysis of cellulose: Analytical description of a mechanistic model. Biotechnol Bioeng 20:637–663.

Sangseethong K, Meunier-Goddik L, Tantasucharit U, Liaw ET, Penner MH. 1998. Rationale for particle size effect on rates of enzymatic saccharification of microcrystalline cellulose. J Food Biochem 22: 321–330.

Scheiding W, Thoma M, Ross A, Schugerl K. 1984. Modeling of the enzymatic hydrolysis of cellobiose and cellulose by a complex enzyme mixture of *Trichoderma reesei* QM9414. Appl Microbiol Biotechnol 20:176–182.

Stalbrand H, Mansfield SD, Saddler JN, Kilburn DG, Warren RAJ, Gilkes NR. 1998. Analysis of molecular size distributions of cellulose molecules during hydrolysis of cellulose by recombinant *Cellulomonas fimi* b-1,4-glucanases. Appl Environ Microbiol 64: 2374–2379.

Steiner W, Sattler W, Esterbauer H. 1988. Adsorption of *Trichoderma reesei* cellulase on cellulose: Experimental data and their analysis by different equations. Biotechnol Bioeng 32:853–865.

Suga K, van Dedem G, Moo-Young M. 1975. Degradation of polysaccharides by endo and exo enzymes: A theoretical analysis. Biotechnol Bioeng 17:433–439.

Tomme P, Van Tilbeurgh H, Pettersson G, Van Damme J, Vandekerckhove J, Knowles J, Teeri TT, Claeyssens M. 1988. Studies of the cellulolytic system of *Trichoderma reesei* QM9414: Analysis of domain function in two cellobiohydrolases by limited proteolysis. Eur J Biochem 170:575–581.

Woodward J, Hayes MK, Lee NE. 1988a. Hydrolysis of cellulose by saturating and non-saturating concentrations of cellulase: implications of synergism. Bio/Technology 6:301–304.

Woodward J, Limat M, Lee NE. 1988b. The role of cellulase concentration in determining the degree of synergism in the hydrolysis of microcrystalline cellulose. Biochem J 255:895–899.

Yang B, Willies DM, Wyman CE. 2006. Changes in the enzymatic hydrolysis rate of Avicel cellulose with conversion. Biotechnol Bioeng 94:1122–1128.

Zhang Y-HP, Lynd LR. 2004. Toward an aggregated understanding of enzymatic hydrolysis of cellulose: Noncomplexed cellulase systems. Biotechnol Bioeng 88:797–824.

Zhang Y-HP, Lynd LR. 2006. A functionally based model for hydrolysis of cellulose by fungal cellulase. Biotechnol Bioeng 94:888–898.

Zhang S, Wolfgang DE, Wilson DB. 1999. Substrate heterogeneity causes the nonlinear kinetics of insoluble cellulose hydrolysis. Biotechnol Bioeng 66:35C41.

Zhou W, Schüttler HB, Hao Z, Xu Y. 2009a. Cellulose hydrolysis in evolving substrate morphologies I: A general modeling formalism. Biotechnol Bioeng 104:261–274.

Zhou W, Hao Z, Xu Y, Schüttler HB. 2009b. Cellulose hydrolysis in evolving substrate morphologies II: Numerical results and analysis. Biotechnol Bioeng 104:275–289.